Dual Role for Inositol-requiring Enzyme 1α in Promoting the Development of Hepatocellular Carcinoma during Diet-induced Obesity

Ying Wu[1,*], Bo Shan[1,*,#], Jianli Dai[1,*], Zhixiong Xia[2], Jie Cai[3], Tianwei Chen[1], Songya Lv[3], Yuxiong Feng[4], Ling Zheng[3], Yan Wang[3], Jianfeng Liu[2], Jing Fang[1], Dong Xie[1], Liangyou Rui[5], Jianmiao Liu[2] and Yong Liu[3]

[1]Key Laboratory of Nutrition and Metabolism, Institute for Nutritional Sciences, Shanghai Institutes for Biological Sciences, Chinese Academy of Sciences; University of the Chinese Academy of Sciences, Shanghai 200031, China

[2]Cellular Signaling Laboratory, Key Laboratory of Molecular Biophysics of Ministry of Education, Huazhong University of Science and Technology, Wuhan 430074, China.

[3]Hubei Key Laboratory of Cell Homeostasis, College of Life Sciences, the Institute for Advanced Studies, Wuhan University, Wuhan 430072, China

[4]Whitehead Institute for Biomedical Research, Nine Cambridge Center, Cambridge, MA 02142, USA

[5]Department of Molecular and Integrative Physiology, the University of Michigan Medical School, Ann Arbor, MI 48109, USA

[*]These authors contributed equally to this work.

[#]Current address: Touchstone Diabetes Center, Department of Internal Medicine, University of Texas Southwestern Medical Center, Dallas, TX 75390, USA

Correspondence: Yong Liu (liuyong31279@whu.edu.cn).

Key words: HCC, Obesity, ER stress, IRE1α, STAT3

Author Manuscript

This is the author manuscript accepted for publication and has undergone full peer review but has not been through the copyediting, typesetting, pagination and proofreading process, which may lead to differences between this version and the Version of record. Please cite this article as doi:10.1002/hep.29871.

This article is protected by copyright. All rights reserved.

Correspondence address:
Yong Liu, Ph.D.
College of Life Sciences, Wuhan University
299 Bayi Road, Wuhan 430072, China
E-mail: liuyong31279@whu.edu.cn
Telephone: +86-27-68753463

Abbreviations:
HCC, hepatocellular carcinoma;
ER, endoplasmic reticulum;
IRE1α, inositol-requiring enzyme 1α;
UPR, unfolded protein response;
DEN, diethylnitrosamine;
NASH, nonalcoholic steatohepatitis;
NAFLD, nonalcoholic fatty-liver disease;
NF-κB, nuclear factor kappa-light-chain-enhancer of activated B cells;
IKK, IκB kinase;
LKO, liver specific *IRE1α* knockout;
TNF, tumor necrosis factor;
IL-6, interleukin 6;
STAT3, signal transducer and activator of transcription 3;
PERK, PKR-like endoplasmic reticulum kinase;
ATF6, activating transcription factor 6;
ATF4, activating transcription factor 4;
XBP1, X-box binding protein 1;
eIF2α, eukaryotic translation initiation factor 2 alpha;
CHOP, C/EBP homologous protein;
DR5, death receptor 5;
Trb3, Tribbles homolog 3;
c-Myc, myelocytomatosis oncogene;
c-Fos, FBJ osteosarcoma oncogene;

This article is protected by copyright. All rights reserved.

Hif1a, hypoxia inducible factor 1, alpha subunit;
Bloc1s1, biogenesis of lysosomal organelles complex-1, subunit 1;
TG, triglycerides;
TUNEL, terminal deoxynucleotidyl transferase dUTP nick end labeling;
BCL2, B-cell lymphoma 2;
TMA, tissue microarray;
TRAF2, TNF-receptor-associated factor 2;
ERN1, endoplasmic reticulum to nucleus signaling 1;
RIDD, IRE1-dependent decay of mRNA.

Financial Support:
This work was supported by grants from the National Natural Science Foundation of China and Ministry of Science and Technology (No. 81420108006, 31690102, 2016YFA0500100, 31230036 and 91539107) to YL and JL.

Author Manuscript

This article is protected by copyright. All rights reserved.

Abstract

Obesity is associated with both endoplasmic reticulum (ER) stress and chronic metabolic inflammation. ER stress activates the unfolded protein response (UPR) and has been implicated in a variety of cancers, including hepatocellular carcinoma (HCC). It is unclear whether individual UPR pathways are mechanistically linked to HCC development, however. Here we report a dual role for inositol-requiring enzyme 1α (IRE1α), the ER-localized UPR signal transducer, in obesity-promoted HCC development. We found that genetic ablation of IRE1α in hepatocytes not only markedly reduced the occurrence of diethylnitrosamine (DEN)-induced HCC in LKO mice when fed a normal chow (NC) diet, but also protected against the acceleration of HCC progression during high-fat diet (HFD) feeding. Irrespective of their adiposity states, LKO mice showed decreased hepatocyte proliferation and STAT3 activation, even in the face of increased hepatic apoptosis. Furthermore, IRE1α abrogation blunted obesity-associated activation of hepatic IKKβ-NF-κB pathway, leading to reduced production of the tumor-promoting inflammatory cytokines TNF and IL-6. Importantly, higher IRE1α expression along with elevated STAT3 phosphorylation was also observed in the tumor tissues from human HCC patients, correlating with their poorer survival rate. *Conclusion*: These results demonstrate that IRE1α acts in a feed-forward loop during obesity-induced metabolic inflammation to promote HCC development through STAT3-mediated hepatocyte proliferation.

Author Manuscript

This article is protected by copyright. All rights reserved.

Author Manuscript

Introduction

Hepatocellular carcinoma (HCC) is the major form of primary liver cancer, which is the second leading cause of cancer deaths owing to its poor 5-year survival rate (1). The initiation and malignant progression of HCC rely upon the complex interactions between genetic, environmental, and lifestyle factors. Human epidemiological studies have established overweight and obesity as a profound carcinogenic risk factor (2), and an up to 4.5-fold increase in relative HCC risk has been documented in male subjects with obesity (3). Given that the global prevalence of obesity is reaching an alarming epidemic proportion with estimated ~300 million obese individuals worldwide (4, 5), such an increase in HCC risk will pose a daunting public health problem. Thus, it is of utmost importance to understand obesity-associated tumor-promoting mechanisms underlying the development of HCC.

A great majority of HCC develops in the context of chronic liver damage arising from exposure to carcinogens, hepatitis viral infections, as well as nonalcoholic steatohepatitis (NASH) (6). NASH is a severe stage of nonalcoholic fatty-liver disease (NAFLD) that is highly associated with obesity (7). Recent studies have revealed several potential mechanisms for the HCC-promoting impact of obesity and NAFLD, including inflammation, endoplasmic reticulum (ER) stress, and oxidative stress (8-13). Proinflammatory cytokines, particularly TNF and IL-6, whose circulating levels are typically elevated in obesity (14), have been shown to play pivotal roles in obesity and NASH promotion of carcinogen-induced HCC development (9). Moreover, both ER and oxidative stresses are known to induce hepatocyte death, resulting in liver damage that stimulates the compensatory proliferation of differentiated hepatocytes (10, 11). During this process, activation of NF-κB as well as STAT3 in initiated hepatocytes is thought to drive the malignant progression of HCC (8, 9). Notably, in chemical carcinogen diethylnitrosamine (DEN)-induced HCC mouse models, TNF signaling was shown to be critical in the promotion by obesity and ER stress of HCC development under the condition of overnutrition (9, 10); however, loss of hepatocyte IKKβ kinase or NF-κB, the downstream component of the canonical TNF pathway, was reported to enhance chemical hepatocarcinogenesis in the absence of obesity (11, 12, 15). Thus, it remains largely obscure whether there exist common mechanisms linking obesity, ER stress, and hepatic inflammatory microenvironment to the malignant progression of HCC.

This article is protected by copyright. All rights reserved.

Author Manuscript

Perturbations of the ER function as a result of excessive accumulation of unfolded/misfolded proteins or alterations in ER lipid compositions lead to ER stress and activation of the adaptive unfolded protein response (UPR) (16, 17). Three ER-localized transmembrane signal transducers, inositol-requiring enzyme 1 (IRE1), PKR-like endoplasmic reticulum kinase (PERK), and activating transcription factor 6 (ATF6), function to govern the cellular UPR program (16). Persistent activation of these ER stress sensors is thought to confer a greater tumorigenic capacity upon malignant cells (18, 19). Although both metabolic ER stress and chronic inflammation have been found in the state of obesity (20-22), it has yet to be dissected if individual UPR branches are directly involved in promoting liver damage, inflammation, and compensatory proliferation during HCC development in the face of obesity. In particular, IRE1 is the most conserved ER stress sensor that possesses both Ser/Thr kinase and endoribonuclease activities (23). Upon ER stress, IRE1 is activated through autophosphorylation and dimerization/oligomerization, and regulates the non-conventional splicing of X-box binding protein 1 (*Xbp1*) mRNA or degrades a select subset of mRNAs via a process termed regulated IRE1-dependent decay (RIDD) (23). Our previous studies in mouse models have revealed that hepatic IRE1α is hyperactivated in the state of obesity (24, 25), and it has an important role during reparative liver regeneration (26). Here we investigated whether IRE1α is able to connect metabolic ER stress to promotion of hepatocyte proliferation and HCC development during overnutrition-induced obesity. We found that IRE1α expression correlated with human HCC, and through its impact upon both the IKKβ-NF-κB and STAT3 pathways, IRE1α could exert dual actions in obesity acceleration of carcinogen-induced HCC development.

This article is protected by copyright. All rights reserved.

Author Manuscript

Materials and Methods

Animals

Liver-specific *IRE1α* knockout (LKO) mice on the C57BL/6 background were generated by intercrossing the *Ern1* floxed (*flox/flox*) mice, in which the exon 2 of the *Ern1* allele was flanked by *loxP* sites, with the Alb-*cre* mice as described previously (26, 27). Mice were maintained at 23±3^{o}C with a humidity of 35±5% under a 12/12-hour dark/light cycle (lights on at 6:30 am), with free access to water and food (Shanghai Laboratory Animal Co. Ltd, Shanghai, China). HCC was induced by intraperitoneal (i.p.) injection with one dose of DEN (#N0725, Sigma Aldrich, St. Louis, MO) at 25 mg/kg in 2-week-old male mice. After 4 weeks, mice were either fed the NC or a high-fat diet (HFD, 60% fat in calories; Research Diets, #D12492, New Brunswick, NJ) for the desired periods of time until being sacrificed. All animal experiments were performed according to protocols approved by the Institutional Animal Care and Use Committee at the Institute for Nutritional Sciences, Shanghai Institutes for Biological Sciences, Chinese Academy of Sciences.

Histologic, TUNEL and immunohistochemical analyses

Sectioned liver tissues were fixed in 10% formalin or embedded in Tissue-Tek OCT compound for paraffin and frozen block preparation, respectively. Paraffin-embedded liver sections were subjected to H&E staining, TUNEL analysis, and immunohistochemistry (IHC). Cellular apoptosis was analyzed using the Dead End TM Fluorometric TUNEL System (Promega Corp., Madison, WI) according to the manufacturer's instructions. Apoptotic signals in liver sections were visualized by fluorescence microscopy. Immunohistochemical analyses of Ki-67, PCNA and K19 were performed. Briefly, liver slices were permeabilized with blocking buffer (5% BSA/0.25% TX-100 in PBS) and incubated with the Ki-67 (#550609, BD Bioscience, San Jose, CA), PCNA (#13110, Cell Signaling Technology, Danvers, MA) or K19 (sc-376126, Santa Cruz, Dallas, Texas) antibody overnight at 4 ^{o}C. After washing with PBS, samples were incubated with HRP-conjugated secondary antibody (Invitrogen, Carlsbad, CA) before analysis by microscopy (PerkinElmer, Waltham, MA). Ki67-, PCNA- and TUNEL-positive cells were quantified using Image J software.

All other materials and methods are described in Supplemental Information.

Statistical analysis

This article is protected by copyright. All rights reserved.

Data are presented as the mean ± standard errors of the mean (s.e.m.). Statistical analysis was conducted using unpaired two-tailed t-test, one-way or two-way analysis of variance (ANOVA), followed by Bonferroni's post test with GraphPad Prism 5.0. $P<0.05$ was considered statistically significant.

Author Manuscript

This article is protected by copyright. All rights reserved.

Author Manuscript

Results

Ablation of hepatocyte IRE1α protects against obesity-promoted HCC development.

Overnutrition has been reported to promote DEN-induced or ER stress-evoked hepatic tumorigenesis in mice maintained on a high-fat diet (HFD) (9, 10). In accordance with these studies, we also observed markedly increased incidence of HCC in DEN-treated male mice following 24 weeks of HFD feeding when compared to those fed a normal chow (NC) diet (**Fig. S1A-C**). Moreover, immunoblot analysis revealed significantly higher phosphorylation levels of hepatic IRE1α, PERK and eIF2α, and elevated expression levels of BiP, in parallel with prominently increased phosphorylation activation of the oncogenic transcription factor STAT3, in livers of HFD-fed DEN-treated mice (**Fig. S1D**). Phos-tag gel analysis of IRE1α (**Fig. S1E**) and RT-PCR assessment of *Xbp1* mRNA splicing (**Fig. S1F**) further affirmed higher activation of liver IRE1α in HFD-fed animals. Thus, during obesity promotion of DEN-induced tumorigenesis, HFD feeding results in hyperactivation of hepatic IRE1 and PERK pathways of the UPR that accompanied increased STAT3 activation. This indicates a potential link between sustained activation of the ER stress sensors and acceleration of HCC progression.

Given that IRE1α activation was increased in livers of HFD-fed HCC-bearing mice, we employed the liver-specific IRE1α knockout (LKO) mouse model (26, 27) to test if hepatocyte IRE1α contributed to the promotion of HCC progression during overnutrition. Intriguingly, following a short-term HFD feeding of 16 weeks, we observed lower liver weight (an indicator of tumor burden) and reduced DEN-induced HCC incidence in male LKO mice than in *flox/flox* control mice (**Fig. S2A-C**). After 24 weeks of feeding, while no HCC tumors were detectable in NC-fed DEN-treated mice, loss of IRE1α markedly blunted HFD-induced development of HCC in LKO mice without affecting their body weight gain as compared to their *flox/flox* counterparts (**Figure 1A-C**). Quantitative analyses revealed that HFD-fed LKO mice had significantly decreased liver weight (by ~40%; **Figure 1D**) and markedly reduced total number (by ~67%) and maximal size (by ~50%) of visible HCC tumors (**Figure 1E**). Further distribution assessment showed that the number of various tumor sizes was all significantly decreased in LKO mice (**Figure 1F**). These results suggest that abrogation of IRE1α in hepatocytes hinders the acceleration of DEN-induced HCC development in the state of dietary obesity.

Abrogation of hepatocyte IRE1α suppresses chemical tumorigenesis in lean mice.

This article is protected by copyright. All rights reserved.

Author Manuscript

Next, we asked if IRE1α is directly involved in DEN-induced tumorigenesis in the absence of overnutrition-induced obesity. When maintained on a NC diet and examined at 40 weeks after DEN administration, lower incidence of HCC was detected in LKO mice relative to their *flox/flox* control animals (**Figure 2A-C**). Quantitative analysis showed that LKO mice had a ~30% reduction in their liver weight (**Figure 2D**) and significant decreases in the number (by ~50%) and maximal size (by ~50%) of HCC tumors (**Figure 2E**). Distribution assessment also revealed significantly fewer HCC tumors of various sizes (**Figure 2F**). Thus, IRE1α in hepatocytes plays a critical role in carcinogen-induced liver tumorigenesis in addition to mediating the promoting effect of obesity upon HCC progression during overnutrition.

Hepatocyte IRE1α ablation results in enhanced hepatic apoptosis.

To explore the mechanisms by which hepatocyte IRE1α exerts its tumor-promoting effect, we first examined if loss of IRE1α could lead to alterations in hepatic ER stress and cell death that may account for the decreased susceptibility of LKO mice to hepatocarcinogenesis. Short-term DEN administration induced an acute hepatic UPR activation in *flox/flox* control mice, as indicated by elevations in eIF2α phosphorylation, BiP protein expression, *Xbp1* mRNA splicing, as well as the mRNA abundance of *Chop* and its target gene *Dr5* (16, 28), and IRE1α deficiency further enhanced these ER stress markers in LKO mice except *Xbp1* mRNA splicing (**Fig. S3A-C**). At 8 weeks after DEN injection when no HCC tumors were detectable in mice maintained either on NC or HFD, LKO livers showed significantly increased PERK and eIF2α phosphorylation levels despite of decreased PERK protein abundance (**Figure 3A**), while exhibiting no significant changes in BiP protein levels. Because hyperactivation of the PERK-eIF2α branch is known to trigger ER stress-associated apoptosis through the ATF4-CHOP cascade (16, 19, 28), we measured the mRNA abundance of *Atf4*, *Chop*, and two CHOP target genes, *Dr5* and *Trb3*, as well as DR5 protein level, which was all elevated in LKO livers (**Figure 3A, B**). These results indicate that loss of IRE1α could cause an overactivation of the PERK-eIF2α branch in DEN-treated livers, leading to enhanced activation of the apoptotic CHOP pathway (19). Indeed, TUNEL analyses revealed that LKO mice, regardless of NC or HFD feeding after DEN injection, had significantly increased apoptotic cells in their livers relative to their *flox/flox* counterparts (**Figure 3C**). Consistently, the anti-apoptotic protein BCL2 decreased, while the cleaved active form of apoptotic Caspase 3 (c-Caspase 3) increased in LKO livers

This article is protected by copyright. All rights reserved.

(**Figure 3D**). Moreover, in NC-fed mice at 40 weeks and HFD-fed mice at 24 weeks after DEN injection when HCC tumors were easily detectable **(Figure 1)**, we detected in HFD-fed animals significantly elevated hepatic *Xbp1* mRNA splicing but an insignificant alteration in the mRNA level of *Bloc1s1* (**Fig. S4A**), a typical RIDD target gene whose cleavage can be temporally separate from *Xbp1* mRNA splicing (29, 30). Whether fed an NC or a HFD, loss of IRE1α led to markedly reduced *Xbp1* mRNA splicing without a significant change in the mRNA abundance of *Bloc1s1* (**Fig. S4A**), and resulted in similarly enhanced activation of the PERK-eIF2α branch and increased apoptosis in LKO livers (**Fig. S4B, C**). Thus, it is possible that the enhanced cell death in LKO livers, if occurring in initiated hepatocytes, might contribute to the protective effect of IRE1α abrogation during DEN-induced tumorigenesis. However, hepatocyte death has been largely documented to stimulate the compensatory proliferation that promotes chemical carcinogenesis in several mouse HCC models (10-12). Therefore, it is more likely that loss of IRE1α could suppress HCC development through other more predominant mechanisms such as blocking the compensatory proliferation of hepatocytes, even in the face of increased hepatic cell death.

Hepatocyte IRE1α abrogation impedes hepatocyte proliferation through blunting STAT3 activation.

We then examined the impact of IRE1α deficiency upon hepatocyte proliferation. Indeed, immunostaining analyses revealed markedly reduced Ki-67-, PCNA- and K19-positive cells in LKO livers from DEN-treated mice when maintained on NC for 40 weeks or on HFD for 24 weeks relative to their *flox/flox* counterparts (**Figure 4A-C**), suggesting decreased hepatocyte proliferation as a result of IRE1α ablation. Given the critical role of persistent STAT3 activation in driving the proliferation and survival of HCC tumor cells (9, 10, 13, 31, 32), we determined the activation states of STAT3. Immunoblot analysis showed that HFD feeding increased the tyrosine phosphorylation levels of hepatic STAT3 in *flox/flox* mice. By contrast, LKO livers exhibited substantially decreased STAT3 phosphorylation irrespective of NC or HFD feeding (**Figure 4D**). Consistently, HFD feeding significantly increased liver mRNA abundance of STAT3 target genes involved in regulating cellular proliferation, *c-Myc*, *c-Fos* and *Hif1a*, which was prominently reduced in NC- or HFD-fed LKO mice (**Figure 4E**). These results indicate that IRE1α acts to promote hepatocyte proliferation and HCC progression through maintaining the activation of the STAT3 pathway, supporting our previous finding that IRE1α could interact

This article is protected by copyright. All rights reserved.

Author Manuscript

with STAT3 and sustain its activation during reparative liver regeneration (26). To gain insight into the mechanism for IRE1α regulation of STAT3 activation, we utilized chemical inhibitors of IRE1α. Interestingly, blocking IRE1α's kinase activity by KIRA6 not only reduced the ER stressor tunicamycin-induced IRE1α phosphorylation and *Xbp1* splicing, but also blunted IL-6-stimulated STAT3 phosphorylation in a dose-dependent manner in HepG2 cells (**Fig. S5A**). By contrast, inhibition of its RNase activity by 4μ8C did not show a discernable effect on STAT3 phosphorylation (**Fig. S5B**). These data further suggest that IRE1α's kinase, but not RNase, activity may be critical in regulating the activation status of STAT3, in accordance with our reported study showing that IRE1α's kinase but not RNase domain is required for interacting with STAT3 (26).

Hepatic IRE1α deficiency alleviates HFD-induced hepatosteatosis and metabolic inflammation.

We further investigated whether hepatocyte IRE1α abrogation prevented obesity-induced acceleration of HCC progression through affecting liver steatosis and metabolic inflammation. HFD feeding for 4 weeks following DEN treatment resulted in higher hepatic lipid and triglyceride levels relative to NC feeding in *flox/flox* mice, and IRE1α ablation significantly reduced this HFD-induced liver steatosis in LKO mice (**Figure 5A, B**). HFD feeding in *flox/flox* mice also led to increased serum and hepatic levels of TNFα and IL-6, which were significantly blunted in LKO animals (**Figure 5C, D**). Given NF-κB as the classical transcriptional regulator that drives the expression of numerous cytokines and chemokines to maintain the tumor-promoting inflammatory microenvironment (9), we examined its activation state in the livers of DEN-treated mice. Indeed, IRE1α ablation blunted HFD-induced increases in hepatic P65 phosphorylation and *Il-6* mRNA abundance in LKO mice (**Figure 5E, F**). These data suggest that hepatocyte IRE1α serves as a crucial promoter of obesity-associated metabolic inflammation to further enhance the IL-6-STAT3 pathway, thus contributing to the acceleration of HCC progression in the state of obesity.

Hepatocyte IRE1α mediates HFD-induced activation of the IKKβ-NF-κB pathway.

TNF receptor signaling has been shown to be required for obesity- or ER stress-promoted HCC development (9, 10). Thus, we wondered if IRE1α could link overnutrition-induced obesity to hepatic activation of the canonical TNF signaling cascade, i.e. the IKKβ-NF-κB pathway, in

This article is protected by copyright. All rights reserved.

Author Manuscript

DEN-treated mice. When maintained on NC diet, hepatocyte IRE1α ablation showed no effects upon the phosphorylation of IKKβ, IκBα and P65, as well as the protein level of IκBα, in livers of DEN-treated LKO mice relative to their *flox/flox* counterparts (**Figure 6A**). By contrast, following 4 weeks of HFD feeding, DEN-treated LKO livers exhibited marked reductions in the phosphorylation of IKKβ, IκBα and P65, along with an increase in IκBα protein level (**Figure 6A**). Consistently, increased cytoplasmic accumulation and decreased nuclear level of P65 protein were seen in LKO livers following HFD-feeding (**Figure 6B**). These data indicate that hepatocyte IRE1α abrogation leads to suppression of obesity-associated activation of hepatic IKKβ-NF-κB pathway.

Then we examined whether IRE1α was able to mediate TNF activation of the IKKβ-NF-κB pathway in a cell-autonomous fashion. NF-κB-activated luciferase reporter assays showed that siRNA knockdown of the expression of IRE1α substantially diminished the stimulation by recombinant TNFα of NF-κB transcription activity in HepG2 cells (**Figure 6C**). Consistently, IRE1α deficiency resulted in marked suppression of TNFα-induced phosphorylation of IKKβ, IκBα and P65, along with elevated protein level of IκBα in HepG2 cells (**Figure 6D**). However, siRNA knockdown of XBP1 expression had no effect on TNFα-stimulated transcriptional activation of NF-κB (**Fig. S6A**), and did not alter the phosphorylation state of IKKβ, IκBα or P65 while causing an appreciable elevation of IRE1α phosphorylation (**Fig. S6B**). These results demonstrate that IRE1α is coupled to TNF signaling to promote NF-κB activation without requiring XBP1 during metabolic inflammation, which most likely resembles the experimental ER stress state giving rise to IRE1α-directed activation of NF-κB (33, 34).

Higher IRE1α expression correlates with STAT3 activation in human HCC.

To understand the clinical relevance of IRE1α in human HCC, we examined the expression of IRE1α in matched non-tumor and tumor samples from HCC patients. Remarkably, we detected higher IRE1α protein levels in nearly all of the 12 HCC tumor samples as compared to their non-tumor control tissues (**Figure 7A**). We then analyzed the relationship between tumor IRE1α expression, STAT3 phosphorylation and the overall survival of HCC patients by tumor microarray (TMA) analysis of 94 HCC patients. TMA assessment also revealed elevated levels of IRE1α protein, as well as higher phosphorylation of STAT3 in HCC tumors relative to their matched non-tumor tissues (**Figure 7B**). Moreover, higher extent of elevations in IRE1α protein

This article is protected by copyright. All rights reserved.

Author Manuscript

levels and in STAT3 activation states significantly correlated with decreased overall survival rate in 18 and 32 HCC patients, respectively (**Figure 7C**). Linear regression analysis also revealed an appreciable association between IRE1α protein and STAT3 activation (r^2=0.409, p<0.0001) in human HCC (**Figure 7D**). These results suggest that IRE1α indeed represents an important aspect linking the UPR activation to the malignant development of human HCC through the STAT3 pathway.

Author Manuscript

This article is protected by copyright. All rights reserved.

Author Manuscript

Discussion

Persistent activation of the UPR pathways is thought to enable cancer cells to better cope with hostile environment and thus have important roles in promoting tumorigenesis (18). Chronic ER stress in metabolic organs is a common feature in obesity (20), but it remains unclear whether the IRE1α branch of the UPR links obesity-associated inflammation to the promotion of chemical carcinogenesis in the liver. Utilizing a mouse HCC model, this study reveals that during HFD-induced obesity, IRE1α in hepatocytes have multi-faceted actions in accelerating the malignant progression of HCC. On one hand, hepatocyte IRE1α promotes obesity-associated activation of the IKKβ-NF-κB pathway, which leads to increased hepatic production of typical pro-inflammatory cytokines such as IL-6; on the other hand, hepatocyte IRE1α serves to maintain the activation of STAT3, thus promoting hepatocyte proliferation. Given that the IL-6-STAT3 pathway is essential in hepatocyte proliferation during obesity-promoted hepatocarcinogenesis (9, 10), our results uncover a critical IRE1α-mediated feed-forward loop for accelerating HCC development through STAT3-promoted proliferation in the context of overnutrition-induced obesity and metabolic inflammation.

Our findings highlight the crucial IRE1α-STAT3 axis in promoting the malignant progression of HCC regardless of the adiposity states. Following DEN administration, hepatocyte IRE1α ablation resulted in diminished STAT3 activation along with reduced hepatocyte proliferation, thus protecting against HCC development not only in HFD-fed obese mice, but also in NC-fed lean mice. This is congruent with our previous finding that hepatic IRE1α could directly interact with STAT3 to maintain its activation, thereby promoting reparative liver regeneration after tissue damage (26). STAT3 is the oncogenic transcription factor that is central in regulating the proliferation and survival of tumor cells (9, 10, 13, 31), and frequent activation of STAT3 has been documented in human HCCs with poor prognosis (35). Many studies have also established that STAT3 can be activated in cancer by a myriad of cellular pathways in addition to IL-6 and its family members (31). Although the precise mechanism by which IRE1α controls STAT3 activation remains to be deciphered, IRE1α's kinase activity appeared to be involved. Targeted disruption of IRE1α-STAT3 association may block the STAT3 pathway and prevent the progression of HCC even in the absence of obesity and metabolic inflammation.

This article is protected by copyright. All rights reserved.

Author Manuscript

Both TNFα and IL-6 signaling pathways have been found to be important in mediating the HCC-promoting effects of obesity and ER stress (9, 10). Our results also reveal that hepatocyte IRE1α is coupled to metabolic inflammation through enhancing TNFα activation of the IKKβ-NF-κB cascade. IRE1α was reported to associate with TNF-receptor-associated factor 2 (TRAF2) (36) and form a complex with IKKβ through TRAF2 to mediate NF-κB activation during experimental ER stress (33, 34). Recent reported studies also suggested that IRE1α's kinase activity was involved in maintaining the basal activity of IKKβ (37, 38). It is likely that during obesity-associated metabolic ER stress, IRE1α could enhance activation of the IKKβ-NF-κB cascade in hepatocytes through similar mechanisms, leading to higher hepatic production of IL-6 and presumably other inflammatory mediators as well (39, 40). While IRE1α ablation resulted in reduced hepatic levels of TNFα and IL-6 during dietary obesity, we did not detect apparent changes in macrophages or T cells from HCC tumors (data not shown). However, it has yet to be further investigated whether IRE1α-deficient hepatocytes could affect the infiltrated immune cells with regard to their capacity of cytokine production to maintain the inflammatory microenvironment in the liver throughout the process of HCC progression. Nevertheless, the reduced production of IL-6 in IRE1α-deficient livers could be a key contributor in diminishing its autocrine activation of STAT3 to blunt the acceleration of HCC in the face of dietary obesity.

It is worth noting that hepatocyte IRE1α ablation resulted in alleviation of hepatosteatosis and liver inflammation during HFD feeding, but led to increased cell death that could be ascribed to hyperactivation of the PERK-eIF2α pathway and/or deficient STAT3 activation in both obese and lean mice. Whereas enhanced apoptosis in transformed hepatocytes of DEN-treated LKO mice might contribute in hindering the progression of HCC, it is more likely that such increased apoptosis was unable to trigger the compensatory proliferation of hepatocytes (41, 42) owing to the impairment of STAT3 activation in IRE1α-deficient hepatocytes. Of interesting note, we also observed a reduction of PERK protein abundance despite of its higher phosphorylation level in IRE1α-deficient hepatocytes. This suggests a possible, as-yet-unrecognized interconnection between these two UPR branches in this particular experimental context. Moreover, given its roles in hepatic lipid metabolism (27, 43), it remains to be fully understood whether the IRE1α-XBP1 branch contributed to, or the IRE1α-STAT3 axis was also involved in, overnutrition-associated hepatosteatosis during obesity-promoted HCC progression.

This article is protected by copyright. All rights reserved.

Finally, we have found high levels of IRE1α expression in association with human HCC tumors, which appreciably correlated with increased STAT3 activation and poorer survival rate of the examined patients. It remains to be dissected, however, what exact activation features enable IRE1α to promote STAT3 activation in human HCC. Interestingly, human cancer genome studies of HCC have uncovered a number of somatic mutations within *ERN1,* the human gene encoding IRE1α (44, 45). Further functional investigations are warranted to delineate the potential impact of these mutations upon its role in maintaining the persistent activation of STAT3 and NF-κB in human HCC, whether it is associated with higher risks endowed by obesity, NASH, or HBV/HCV infection. In short, our work demonstrates a crucial tumor-promoting activity of IRE1α in HCC development. A variety of human cancer has been documented to have increased ER stress (19). Given the essential importance of STAT3 and NF-κB in other inflammation-associated cancers (9, 46-50), IRE1α may contribute to the malignant progression of other types of tumor as well. Targeted blocking of the molecular connections between IRE1α and STAT3 or IKKβ may bear promising translational potentials for the development of therapeutics against not only HCC but also many other malignancies.

Author Manuscript

This article is protected by copyright. All rights reserved.

Author Manuscript

References

1. Torre LA, Bray F, Siegel RL, Ferlay J, Lortet-Tieulent J, Jemal A. Global cancer statistics, 2012. CA Cancer J Clin 2015;65:87-108.

2. Calle EE, Kaaks R. Overweight, obesity and cancer: epidemiological evidence and proposed mechanisms. Nat Rev Cancer 2004;4:579-591.

3. Calle EE, Teras LR, Thun MJ. Obesity and mortality. N Engl J Med 2005;353:2197-2199.

4. Ng M, Fleming T, Robinson M, Thomson B, Graetz N, Margono C, Mullany EC, et al. Global, regional, and national prevalence of overweight and obesity in children and adults during 1980-2013: a systematic analysis for the Global Burden of Disease Study 2013. Lancet 2014;384:766-781.

5. Ellulu M, Abed Y, Rahmat A, Ranneh Y, Ali F. Epidemiology of obesity in developing countries: challenges and prevention. Global Epidemic Obesity 2014;2.

6. El-Serag HB, Rudolph KL. Hepatocellular carcinoma: epidemiology and molecular carcinogenesis. Gastroenterology 2007;132:2557-2576.

7. Cohen JC, Horton JD, Hobbs HH. Human fatty liver disease: old questions and new insights. Science 2011;332:1519-1523.

8. Font-Burgada J, Sun B, Karin M. Obesity and Cancer: The Oil that Feeds the Flame. Cell Metab 2016;23:48-62.

9. Park EJ, Lee JH, Yu GY, He G, Ali SR, Holzer RG, Osterreicher CH, et al. Dietary and genetic obesity promote liver inflammation and tumorigenesis by enhancing IL-6 and TNF expression. Cell 2010;140:197-208.

10. **Nakagawa H**, **Umemura A**, Taniguchi K, Font-Burgada J, Dhar D, Ogata H, Zhong Z, et al. ER stress cooperates with hypernutrition to trigger TNF-dependent spontaneous HCC development. Cancer Cell 2014;26:331-343.

11. Fausto N. Mouse liver tumorigenesis: models, mechanisms, and relevance to human disease. Semin Liver Dis 1999;19:243-252.

12. Sakurai T, He G, Matsuzawa A, Yu GY, Maeda S, Hardiman G, Karin M. Hepatocyte necrosis induced by oxidative stress and IL-1 alpha release mediate carcinogen-induced compensatory proliferation and liver tumorigenesis. Cancer Cell 2008;14:156-165.

This article is protected by copyright. All rights reserved.

13. **He G**, **Yu GY**, Temkin V, Ogata H, Kuntzen C, Sakurai T, Sieghart W, et al. Hepatocyte IKKbeta/NF-kappaB inhibits tumor promotion and progression by preventing oxidative stress-driven STAT3 activation. Cancer Cell 2010;17:286-297.

14. Weisberg SP, McCann D, Desai M, Rosenbaum M, Leibel RL, Ferrante AW, Jr. Obesity is associated with macrophage accumulation in adipose tissue. J Clin Invest 2003;112:1796-1808.

15. Sakurai T, Maeda S, Chang L, Karin M. Loss of hepatic NF-kappa B activity enhances chemical hepatocarcinogenesis through sustained c-Jun N-terminal kinase 1 activation. Proc Natl Acad Sci U S A 2006;103:10544-10551.

16. Walter P, Ron D. The unfolded protein response: from stress pathway to homeostatic regulation. Science 2011;334:1081-1086.

17. Hetz C. The unfolded protein response: controlling cell fate decisions under ER stress and beyond. Nat Rev Mol Cell Biol 2012;13:89-102.

18. Cubillos-Ruiz JR, Bettigole SE, Glimcher LH. Tumorigenic and Immunosuppressive Effects of Endoplasmic Reticulum Stress in Cancer. Cell 2017;168:692-706.

19. Wang M, Kaufman RJ. The impact of the endoplasmic reticulum protein-folding environment on cancer development. Nat Rev Cancer 2014;14:581-597.

20. Hotamisligil GS. Endoplasmic reticulum stress and the inflammatory basis of metabolic disease. Cell 2010;140:900-917.

21. **Shan B**, **Wang X**, **Wu Y**, Xu C, Xia Z, Dai J, Shao M, et al. The metabolic ER stress sensor IRE1alpha suppresses alternative activation of macrophages and impairs energy expenditure in obesity. Nat Immunol 2017;18:519-529.

22. Qiu Y, Shan B, Yang L, Liu Y. Adipose tissue macrophage in immune regulation of metabolism. Sci China Life Sci 2016;59:1232-1240.

23. Hetz C, Martinon F, Rodriguez D, Glimcher LH. The unfolded protein response: integrating stress signals through the stress sensor IRE1alpha. Physiol Rev 2011;91:1219-1243.

24. **Mao T**, **Shao M**, Qiu Y, Huang J, Zhang Y, Song B, Wang Q, et al. PKA phosphorylation couples hepatic inositol-requiring enzyme 1alpha to glucagon signaling in glucose metabolism. Proc Natl Acad Sci U S A 2011;108:15852-15857.

25. **Jiang S**, **Yan C**, Fang QC, Shao ML, Zhang YL, Liu Y, Deng YP, et al. Fibroblast growth factor 21 is regulated by the IRE1alpha-XBP1 branch of the unfolded protein response and

Author Manuscript

This article is protected by copyright. All rights reserved.

counteracts endoplasmic reticulum stress-induced hepatic steatosis. J Biol Chem 2014;289:29751-29765.

26. **Liu Y**, **Shao M**, Wu Y, Yan C, Jiang S, Liu J, Dai J, et al. Role for the endoplasmic reticulum stress sensor IRE1alpha in liver regenerative responses. J Hepatol 2015;62:590-598.

27. **Shao M**, **Shan B**, Liu Y, Deng Y, Yan C, Wu Y, Mao T, et al. Hepatic IRE1alpha regulates fasting-induced metabolic adaptive programs through the XBP1s-PPARalpha axis signalling. Nat Commun 2014;5:3528.

28. **Lu M**, **Lawrence DA**, Marsters S, Acosta-Alvear D, Kimmig P, Mendez AS, Paton AW, et al. Opposing unfolded-protein-response signals converge on death receptor 5 to control apoptosis. Science 2014;345:98-101.

29. Maurel M, Chevet E, Tavernier J, Gerlo S. Getting RIDD of RNA: IRE1 in cell fate regulation. Trends Biochem Sci 2014;39:245-254.

30. Bright MD, Itzhak DN, Wardell CP, Morgan GJ, Davies FE. Cleavage of BLOC1S1 mRNA by IRE1 Is Sequence Specific, Temporally Separate from XBP1 Splicing, and Dispensable for Cell Viability under Acute Endoplasmic Reticulum Stress. Mol Cell Biol 2015;35:2186-2202.

31. Yu H, Lee H, Herrmann A, Buettner R, Jove R. Revisiting STAT3 signalling in cancer: new and unexpected biological functions. Nat Rev Cancer 2014;14:736-746.

32. **Bard-Chapeau EA**, **Li S**, Ding J, Zhang SS, Zhu HH, Princen F, Fang DD, et al. Ptpn11/Shp2 acts as a tumor suppressor in hepatocellular carcinogenesis. Cancer Cell 2011;19:629-639.

33. Kaneko M, Niinuma Y, Nomura Y. Activation signal of nuclear factor-kappa B in response to endoplasmic reticulum stress is transduced via IRE1 and tumor necrosis factor receptor-associated factor 2. Biol Pharm Bull 2003;26:931-935.

34. **Hu P**, **Han Z**, Couvillon AD, Kaufman RJ, Exton JH. Autocrine tumor necrosis factor alpha links endoplasmic reticulum stress to the membrane death receptor pathway through IRE1alpha-mediated NF-kappaB activation and down-regulation of TRAF2 expression. Mol Cell Biol 2006;26:3071-3084.

35. Calvisi DF, Ladu S, Gorden A, Farina M, Conner EA, Lee JS, Factor VM, et al. Ubiquitous activation of Ras and Jak/Stat pathways in human HCC. Gastroenterology 2006;130:1117-1128.

This article is protected by copyright. All rights reserved.

Author Manuscript

36. Urano F, Wang X, Bertolotti A, Zhang Y, Chung P, Harding HP, Ron D. Coupling of stress in the ER to activation of JNK protein kinases by transmembrane protein kinase IRE1. Science 2000;287:664-666.

37. Tam AB, Mercado EL, Hoffmann A, Niwa M. ER stress activates NF-kappaB by integrating functions of basal IKK activity, IRE1 and PERK. PLoS One 2012;7:e45078.

38. **Keestra-Gounder AM**, **Byndloss MX**, Seyffert N, Young BM, Chavez-Arroyo A, Tsai AY, Cevallos SA, et al. NOD1 and NOD2 signalling links ER stress with inflammation. Nature 2016;532:394-397.

39. Zhang K, Kaufman RJ. From endoplasmic-reticulum stress to the inflammatory response. Nature 2008;454:455-462.

40. Hummasti S, Hotamisligil GS. Endoplasmic reticulum stress and inflammation in obesity and diabetes. Circ Res 2010;107:579-591.

41. Luedde T, Kaplowitz N, Schwabe RF. Cell death and cell death responses in liver disease: mechanisms and clinical relevance. Gastroenterology 2014;147:765-783 e764.

42. **Vucur M**, **Reisinger F**, Gautheron J, Janssen J, Roderburg C, Cardenas DV, Kreggenwinkel K, et al. RIP3 inhibits inflammatory hepatocarcinogenesis but promotes cholestasis by controlling caspase-8- and JNK-dependent compensatory cell proliferation. Cell Rep 2013;4:776-790.

43. So JS, Hur KY, Tarrio M, Ruda V, Frank-Kamenetsky M, Fitzgerald K, Koteliansky V, et al. Silencing of lipid metabolism genes through IRE1alpha-mediated mRNA decay lowers plasma lipids in mice. Cell Metab 2012;16:487-499.

44. Greenman C, Stephens P, Smith R, Dalgliesh GL, Hunter C, Bignell G, Davies H, et al. Patterns of somatic mutation in human cancer genomes. Nature 2007;446:153-158.

45. **Guichard C**, **Amaddeo G**, **Imbeaud S**, Ladeiro Y, Pelletier L, Maad IB, Calderaro J, et al. Integrated analysis of somatic mutations and focal copy-number changes identifies key genes and pathways in hepatocellular carcinoma. Nat Genet 2012;44:694-698.

46. Sansone P, Storci G, Tavolari S, Guarnieri T, Giovannini C, Taffurelli M, Ceccarelli C, et al. IL-6 triggers malignant features in mammospheres from human ductal breast carcinoma and normal mammary gland. J Clin Invest 2007;117:3988-4002.

Author Manuscript

This article is protected by copyright. All rights reserved.

47. Gao SP, Mark KG, Leslie K, Pao W, Motoi N, Gerald WL, Travis WD, et al. Mutations in the EGFR kinase domain mediate STAT3 activation via IL-6 production in human lung adenocarcinomas. J Clin Invest 2007;117:3846-3856.

48. **Bollrath J**, **Phesse TJ**, von Burstin VA, Putoczki T, Bennecke M, Bateman T, Nebelsiek T, et al. gp130-mediated Stat3 activation in enterocytes regulates cell survival and cell-cycle progression during colitis-associated tumorigenesis. Cancer Cell 2009;15:91-102.

49. **Grivennikov S**, **Karin E**, **Terzic J**, Mucida D, Yu GY, Vallabhapurapu S, Scheller J, et al. IL-6 and Stat3 are required for survival of intestinal epithelial cells and development of colitis-associated cancer. Cancer Cell 2009;15:103-113.

50. **Pikarsky E**, **Porat RM**, **Stein I**, Abramovitch R, Amit S, Kasem S, Gutkovich-Pyest E, et al. NF-kappaB functions as a tumour promoter in inflammation-associated cancer. Nature 2004;431:461-466.

Author Manuscript

This article is protected by copyright. All rights reserved.

Author Manuscript

AUTHOR CONTRIBUTIONS

Y.W, B.S and Y.L conceived and designed the studies. Y.W, B.S and J.D performed most of the experiments and analyzed the data. Z.X and J.C conducted some of the animal studies and cell experiments. T.C assisted with analysis of the TMA data. S.L, Y.F, L.Z, Yan.W, Jianfeng.L., J.F, D.X, L.R, and Jianmiao.L provided essential reagents and assisted with the experimental design and data analysis. Y.W, B.S and Y.L wrote the manuscript.

AUTHOR INFORMATION

The authors declare no competing financial interests.

Correspondence and requests for materials should be addressed to Yong Liu (liuyong31279@whu.edu.cn).

This article is protected by copyright. All rights reserved.

Author Manuscript

Figure Legends

Figure 1. LKO mice are protected against obesity-promoted HCC development.

Two-week-old male LKO mice and their *flox/flox* littermates were i.p. injected with DEN (50 mg/kg body weight) and were maintained on an NC (n=8 per genotype) or fed an HFD beginning at 6 weeks of age (n=12 for LKO, n=15 for *flox/flox*). Mice were sacrificed at 30 weeks of age for HCC analysis. (**A**) Body weight. (**B**) Representative images of mouse livers from the indicated group. (**C**) H&E staining of livers. Tumor (T) regions were indicated by circles. Scale bars, 100 μm. (**D**) Ratio of liver weight to body weight. (**E**) Number and maximal size by diameter of liver tumors. (**F**) Number of liver tumors of various sizes. Data in (**D-F**) are shown as the mean ± s.e.m., $*P < 0.05$ by two-tailed unpaired Student's *t*-test or two-way ANOVA.

Figure 2. Hepatocyte IRE1α deletion suppresses HCC development in NC-fed lean LKO mice.

Two-week-old LKO mice and *flox/flox* littermates were i.p. injected with DEN (50 mg/kg body weight) and then maintained on an NC diet (n=12 per genotype), Mice were sacrificed at 42 weeks of age for HCC analysis. (**A**) Schematic of the experimental design. (**B**) Representative images of mouse livers from the indicated genotype. (**C**) H&E staining of livers. Tumor (T) regions were indicated by circles. Scale bars, 100 μm. (**D**) Ratio of liver weight to body weight. (**E**) Number and maximal size of tumors. (**F**) Number of liver tumors of the indicated sizes. Data in (**D-F**) are shown as the mean ± s.e.m., $*P < 0.05$, $**P < 0.01$ by two-tailed unpaired Student's *t*-test or one-way ANOVA.

Figure 3. IRE1α deficiency results in an overactivation of the PERK-eIF2α pathway with increased hepatic apoptosis.

Two-week-old male LKO and *flox/flox* mice injected with DEN were either maintained on an NC or an HFD for 8 weeks (n=8 per group). (**A**) Immunoblot analysis of the phosphorylation of PERK and eIF2α as well as the protein level of BiP and DR5 from liver extracts. Representative immunoblots are shown for three individual mice per group. Shown also are densitometric quantification results after normalization to that of *flox/flox* mice. (**B**) Quantitative RT-PCR analysis of the indicated genes in livers. (**C**) Analysis of apoptosis in liver sections. Shown are representative TUNEL labeling images (6 images per liver) and quantifications of TUNEL-

This article is protected by copyright. All rights reserved.

positive cells (n=5 per group). Scale bars, 100 μm. (**D**) Immunoblot analysis of liver BCL2, pro-Caspase-3 and c-Caspase-3 proteins with densitometric quantifications. Data are shown as the mean ± s.e.m, *$P < 0.05$, ***$P<0.001$ by two-tailed unpaired Student's *t*-test.

Figure 4. Loss of IRE1α impairs hepatocyte proliferation and hepatic STAT3 activation.
Two-week-old male LKO and *flox/flox* mice were injected with DEN and then maintained on an NC for 40 weeks or fed an HFD for 24 weeks, beginning at 6 weeks of age (n=8 per group). (**A, B, C**) Representative immunohistochemistry (IHC) images of livers stained with anti-Ki67 (**A**), anti-PCNA (**B**) or anti-K19 (**C**) antibody (6 images per liver; n=5 per group). Scale bars, 50 μm. Ki67-positive and PCNA-positive cells were quantified and are shown in percentages, respectively. (**D**) Immunoblot analysis of liver IRE1α protein and STAT3 tyrosine phosphorylation. Averaged p-STAT3/STAT3 ratios are shown after normalization to that of NC-fed *flox/flox* mice. (**E**) Quantitative RT-PCR analysis of the indicated STAT3 target genes in the livers. All data are shown as the mean ± s.e.m., *$P < 0.05$, ***$P<0.001$ by two-way ANOVA.

Figure 5. Loss of hepatic IRE1α attenuates HFD-induced hepatic steatosis and inflammation.
Male LKO and *flox/flox* mice injected with DEN were either maintained on an NC or an HFD for 4 weeks (n=8 per group). (**A**) Representative images of livers stained with Oil-red O (10 images per liver; n=5 per group). Scale bars, 100 μm. (**B**) Liver TG content. (**C**) Circulating levels of TNFα and IL-6. (**D**) Liver levels of TNFα and IL-6. (**E**) Immunoblot analysis of liver IRE1α protein and phosphorylation of NF-κB P65 subunit. Shown are representative results of three individual mice from each group. GAPDH was used as the loading control. Phosphorylation levels of P65 were determined by densitometric quantification of the immunoblots, and averaged p-P65/P65 ratios are shown after normalization to that of NC-fed *flox/flox* mice. (**F**) Relative *Il6* mRNA abundance in the livers. Results in (**B-F**) are shown as the mean ± s.e.m., *$P < 0.05$, **$P<0.01$, ***$P<0.001$ by two-way ANOVA.

Figure 6. IRE1α deficiency resulted in suppression of the inflammatory IKKβ-NF-κB pathway.

This article is protected by copyright. All rights reserved.

Author Manuscript

(**A-B**) Hepatocyte IRE1α ablation reduced the activation of hepatic IKKβ pathway in HFD-fed mice. DEN-treated male LKO and *flox/flox* mice were either maintained on an NC or an HFD for 4 weeks (n=8 per group). (**A**) Immunoblot analysis of phosphorylation of IKKβ, IκBα, and P65 in liver extracts. Representative results are shown for three individual mice from each group. Averaged phosphorylation levels were determined by densitometric quantification after normalization to that of *flox/flox* mice. (**B**) Immunoblot analysis of the cytoplasmic and nuclear P65 protein levels in livers of HFD-fed mice. GAPDH or Lamin A/C was used as the loading control for the cytoplasmic or nuclear fractions. The densitometric quantification results are also shown. (**C-D**) Knockdown of IRE1α expression attenuated TNFα-activated IKKβ-NF-κB pathway. (**C**) HepG2 cells were co-transfected for 48 hours with the NF-κB-luciferase reporter plasmid along with two siRNAs directed against IRE1α or a scramble control. Cells were then treated with TNFα (10 ng/ml) for 24 hours, and NF-κB activity was determined by the luciferase assay. Shown are relative luciferase activities after normalization to Renilla that was used as the internal control. (**D**) HepG2 cells were likewise transfected with the two IRE1α siRNAs and then treated with TNFα (10 ng/ml) for the indicated time intervals. Phosphorylation of IKKβ, IκBα and P65 proteins was analyzed and shown after normalization to the value of the untreated control cells (n=4 independent experiments). All data are presented as the mean ± s.e.m., $*P < 0.05$, $**P < 0.01$, $***P < 0.001$ by two-tailed unpaired Student's *t*-test or two-way ANOVA.

Figure 7. IRE1α correlates with STAT3 activation and HCC in human patients.

(**A**) Immunoblot analysis of IRE1α protein in extracts of paired tumor (T) versus non-tumor (N) samples from 12 human HCC patients. (**B-D**) Tumor microarray (TMA) analysis. (**B**) Representative images of IHC staining of IRE1α protein and phosphorylated STAT3 in paired non-HCC and HCC tissue slides from human patients (n=83 patients). Scale bars, 20 μm. (**C**) Kaplan-Meier analysis (log-rank test) of the overall survival of human HCC patients in relation with high (n=18) or low (n=76) expression levels of IRE1α protein and with high (n=32) or low (n=62) levels of phosphorylated STAT3. The *P*-value, hazard ratio (HR) and 95% confidence interval (CI, in brackets) are indicated. (**D**) Linear regression analysis of IRE1α protein expression and STAT3 phosphorylation in HCC tumors. The coefficient of determination (r^2) and *P*-value are indicated.

This article is protected by copyright. All rights reserved.

Author Manuscript

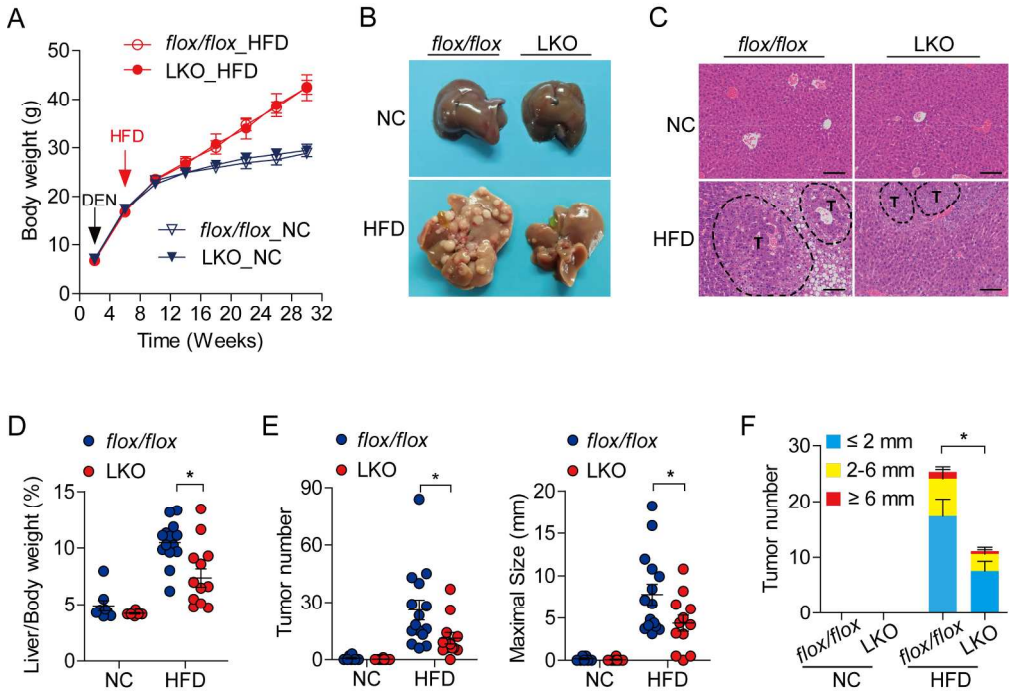

Figure 1. LKO mice are protected against obesity-promoted HCC development.

206x145mm (300 x 300 DPI)

Author M

This article is protected by copyright. All rights reserved.

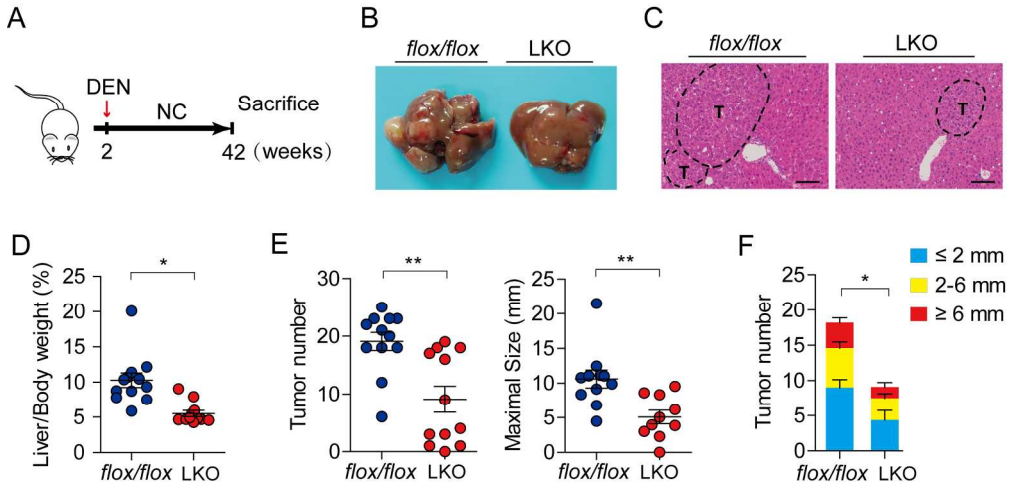

Figure 2. Hepatocyte IRE1α deletion suppresses HCC development in NC-fed lean LKO mice.

197x99mm (300 x 300 DPI)

Author Ma

This article is protected by copyright. All rights reserved.

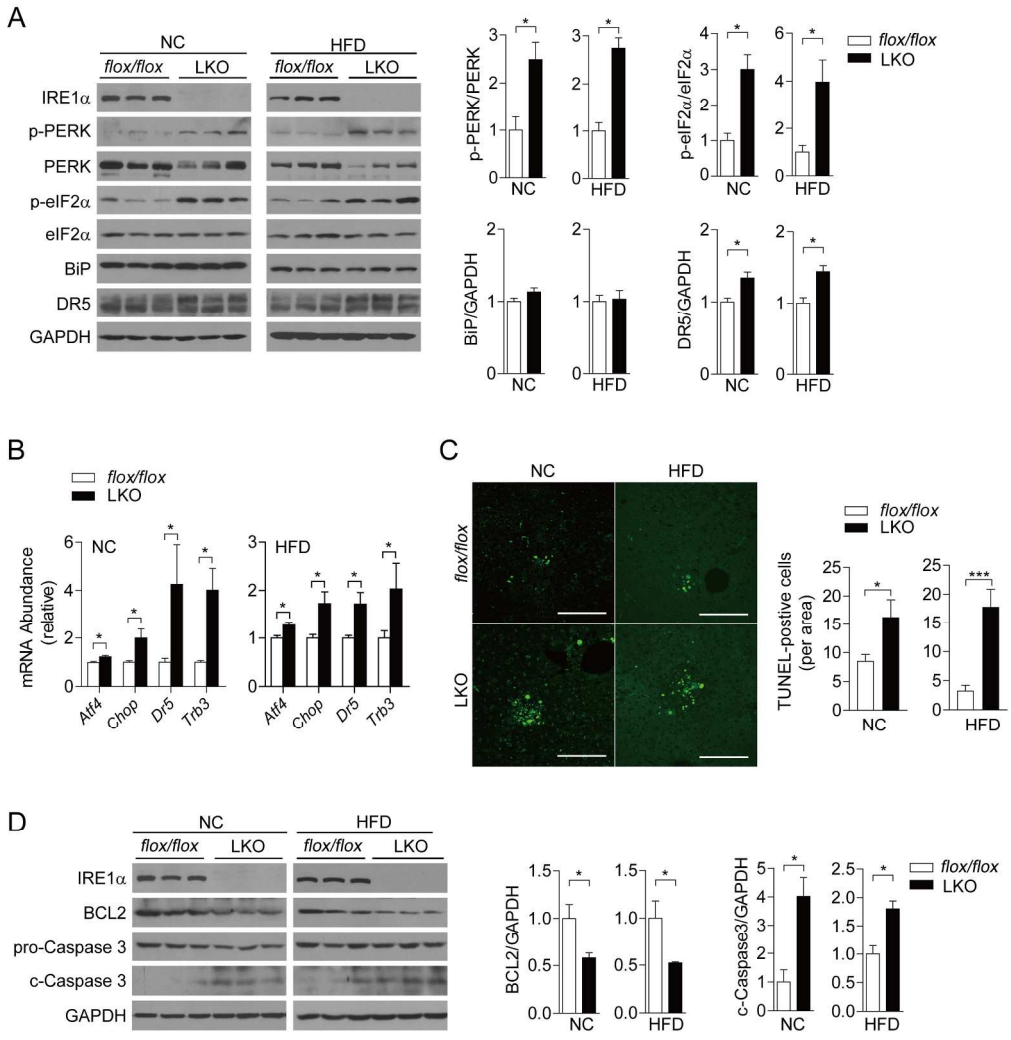

Figure 3. IRE1α deficiency results in an overactivation of the PERK-eIF2α pathway with increased hepatic apoptosis.

204x210mm (300 x 300 DPI)

Auth

This article is protected by copyright. All rights reserved.

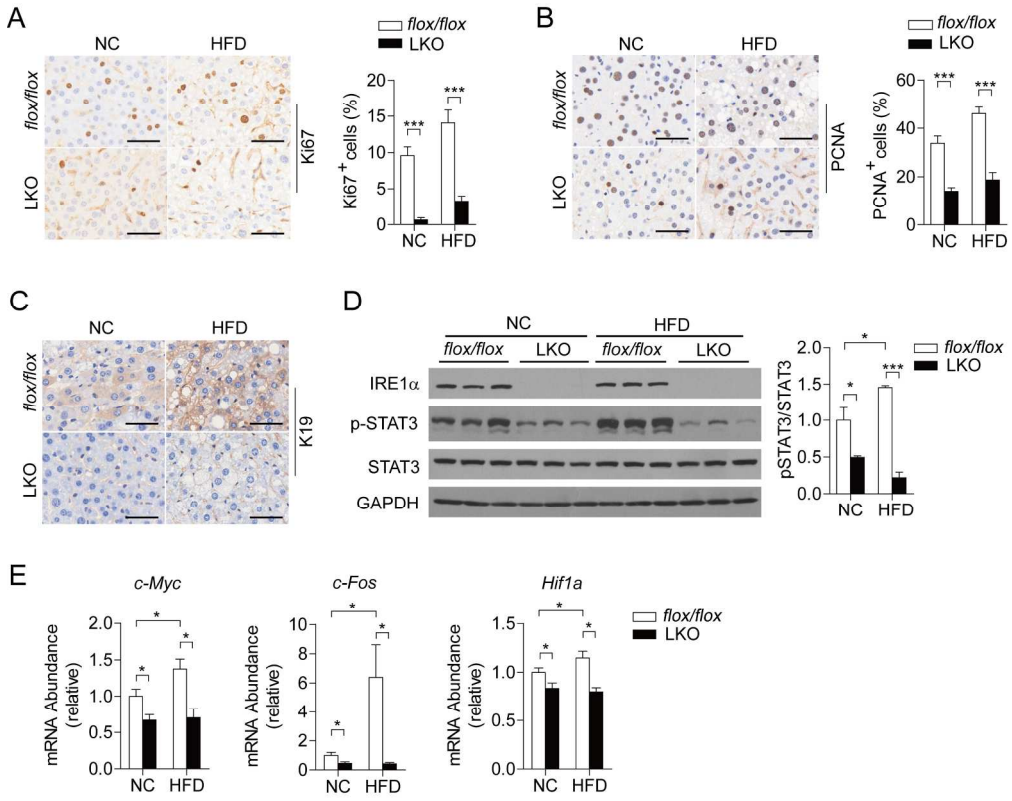

Figure 4. Loss of IRE1α impairs hepatocyte proliferation and hepatic STAT3 activation.

200x162mm (300 x 300 DPI)

Author

This article is protected by copyright. All rights reserved.

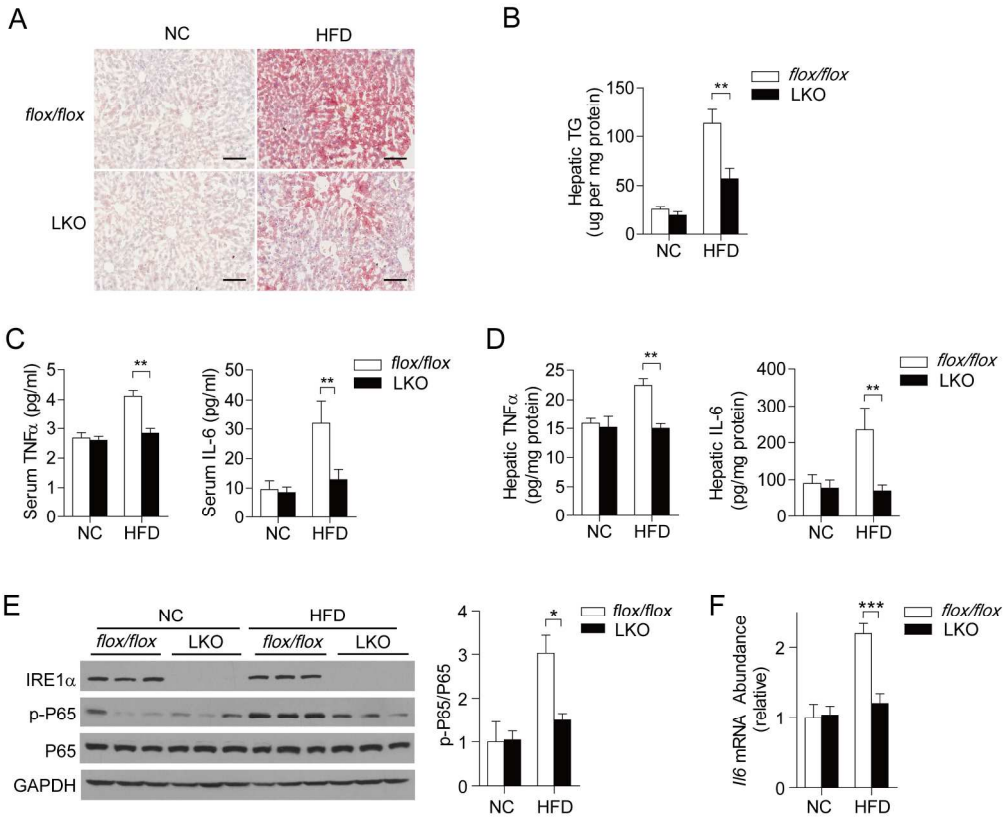

Figure 5. Loss of hepatic IRE1α attenuates HFD-induced hepatic steatosis and inflammation.

199x162mm (300 x 300 DPI)

Author

This article is protected by copyright. All rights reserved.

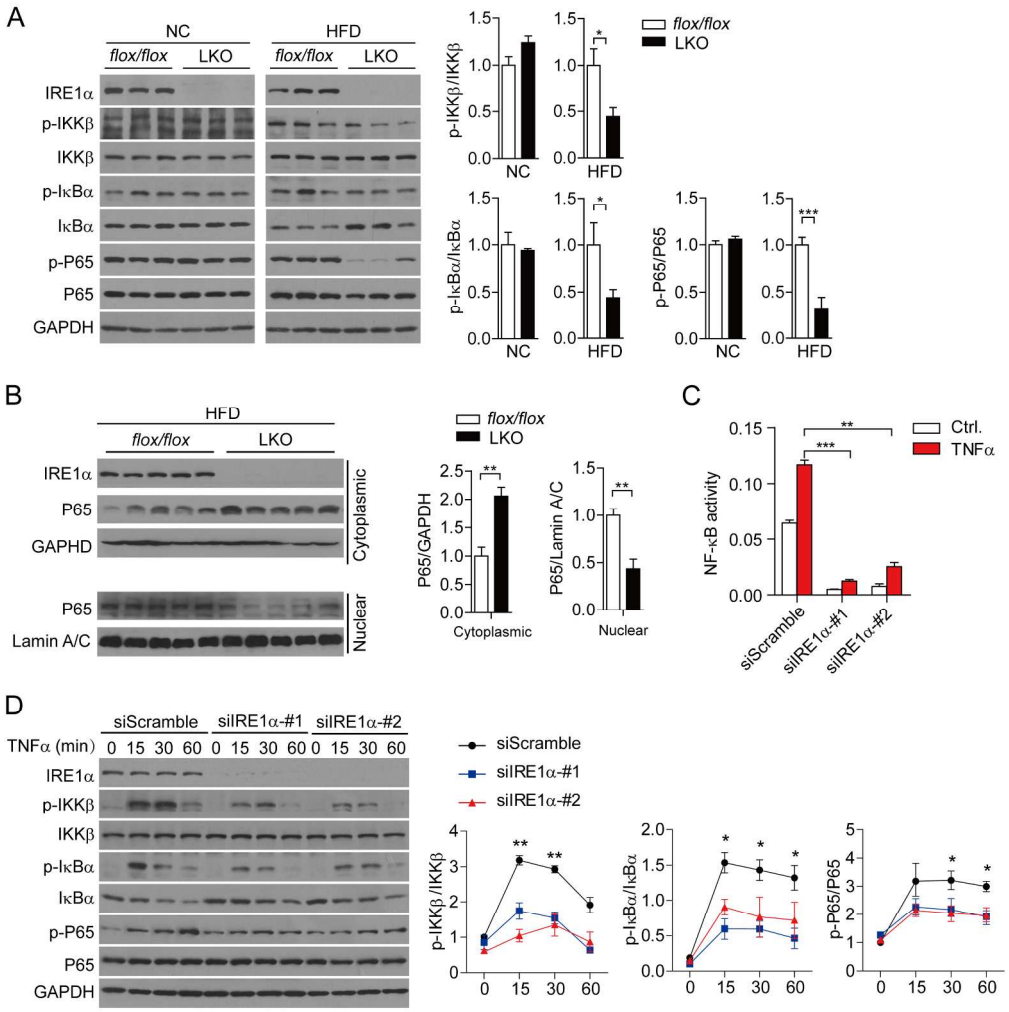

Figure 6. IRE1α deficiency resulted in suppression of the inflammatory IKKβ-NF-κB pathway.

206x208mm (300 x 300 DPI)

Auth

This article is protected by copyright. All rights reserved.

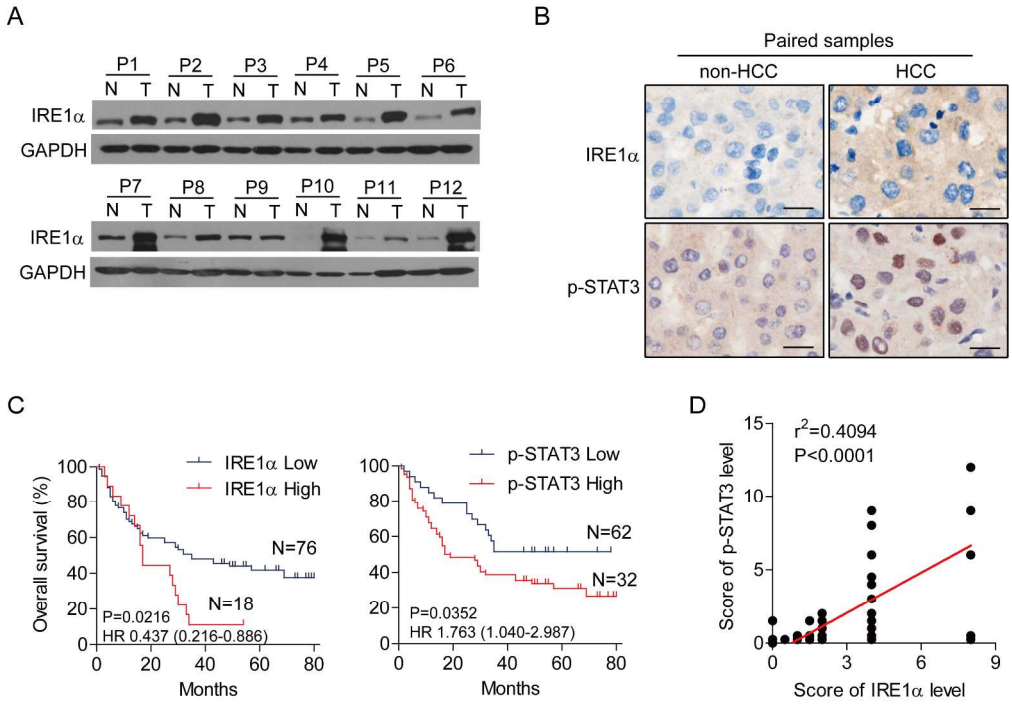

Figure 7. IRE1α correlates with STAT3 activation and HCC in human patients.

224x156mm (300 x 300 DPI)

Author M

This article is protected by copyright. All rights reserved.

Author Manuscript

Supplemental Information

Materials and Methods

Animals

Liver-specific *IRE1α* knockout (LKO) and *flox/flox*) mice (1, 2) were subjected to HCC induction (3). For analysis of DEN-induced liver apoptosis and ER stress, 4-week-old mice were injected i.p. with one dose of DEN at 100 mg/kg. Immunohistochemical analyses of Ki-67, PCNA and K19 were performed as described (4, 5). All animal experiments were performed according to protocols approved by the Institutional Animal Care and Use Committee at the Institute for Nutritional Sciences, Shanghai Institutes for Biological Sciences, Chinese Academy of Sciences.

Oil-red O staining

Frozen liver sections (10 mm) were fixed in formalin and then rinsed with 60% isopropanol. After staining with freshly prepared Oil-red O solution for 10 min, the sections were rinsed again with 60% isopropanol, and nuclei were stained with alum haematoxylin before analysis by microscopy (PerkinElmer, Waltham, MA).

Serum and liver measurements

Serum levels of IL-6 and TNFα were measured using the Interleukin-6 and TNFα ELISA Kit (#KMC0061 and #BMS607HS, ThermoFisher, Waltham, MA), respectively, following the manufacturer's instructions. To determine hepatic levels of IL-6 and TNFα, liver tissues were homogenized by sonication in the homogenization buffer (0.01 N HCl, 1 mM EDTA, 4 mM $Na_2S_2O_5$), and the cellular debris was pelleted by centrifugation at 13,000 rpm for 15 min at 4°C. The homogenates were collected and stored at -80°C prior to measurement by ELISA. Hepatic TGs were analyzed as previously described (2). Briefly, 40-50 mg of liver tissues were homogenized in PBS and mixed with $CHCl_3$-CH_3OH (2:1, v/v). The organic phase was transferred, air-dried overnight, and re-suspended in 1% Triton X-100 in absolute ethanol. The concentration of TGs was determined using the serum triglyceride

This article is protected by copyright. All rights reserved.

Author Manuscript

determination kit (#TR0100, Sigma-Aldrich, St. Louis, MO). All liver measurements were normalized to the total tissue protein concentrations.

Antibodies, chemicals and immunoblotting analysis

Antibodies against IRE1α (#3294), p-eIF2α (#9721), eIF2α (#9722), p-PERK (#3179), PERK (#3192), BiP (#3183), DR5 (#8074), Caspase 3 (#9662), BCL2 (#3498), p-STAT3 (#8204), STAT3 (#14047), p-P65 (#3303), P65 (#3304), P-IκBα (#5209), p-IKKβ (#2697), IKKβ (#8943) and Lamin A/C (#2032) were all from Cell Signaling Technology (Danvers, MA). Antibody (#NB 100-2323) against phosphorylated IRE1α at Ser724 (p-IRE1α) was from Novus Biologicals (Littleton, CO). IκBα (ab32518) antibody was from Abcam (Cambridge, MA), and GAPDH antibody from Kangcheng Biotechnology (Shanghai, China). GAPDH antibody was used at 1:10,000, and all other antibodies were diluted 1:1000. Tunicamycin (#T7765) was purchased from Sigma Aldrich (St. Louis, MO). KIRA (#6532281), an IRE1α kinase inhibitor (6), was from Calbiochem, Merck KGaA (Darmstadt, Germany), and 4μ8C, an inhibitor of IRE1α RNase activity (7, 8), was synthesized in-house at Shanghai Institute of Materia Medica, Chinese Academy of Sciences.

For immunoblotting, tissue or cell lysates were prepared by RIPA buffer (150 mM NaCl, 1% NP-40, 0.5% sodium deoxycholate, 0.1% SDS, 50 mM Tris-HCl, pH 7.4). Nuclear extracts were prepared using the NE-PER Nuclear and Cytoplasmic Extraction Kit (#78833, Thermo Fisher Scientific, Waltham, MA). Protein extracts were separated by SDS-polyacrylamide gel electrophoresis (SDS-PAGE) and transferred onto a polyvinylidene difluoride (PVDF) membrane filter. After incubation with the desired antibodies, the blots were developed with Thermo Scientific's SuperSignal West Pico Chemiluminescent substrate or Millipore's Immunobilon Western Chemiluminescent HRP substrate.

Phos-tag gel analysis was carried out as described (9). Briefly, a 6% SDS-PAGE gel with 25 mM phos-tag was prepared according to the manufacturer's instructions (Phos-tag acrylamide AAL-107, Wako Pure Chemical Industries). IRE1α antibody (#3294, Cell Signaling Technology, Danvers, MA) was used to detect the phosphorylated and non-phosphorylated forms of the IRE1α protein.

This article is protected by copyright. All rights reserved.

Author Manuscript

Quantitative RT-PCR analysis

For quantitative RT-PCR analysis, total RNA was isolated from liver tissues or cells by TRIzol reagent (#T9424, Invitrogen, Carlsbad, CA), and cDNA was synthesized using M-MLV reverse transcriptase and random hexamer primers (#28025013, Thermo Fisher Scienctific, Waltham, MA). Real-time PCR was performed using the SYBR Green PCR system (#4309155, Applied Biosystems, Waltham, MA). *Gapdh* was utilized as an internal control for normalization. The oligonucleotide primers used are as follows:

mouse *Atf4*, forward primer 5'-CCTTCGACCAGTCGGGTTTG-3' and reverse primer 5'-CTGTCCCGGAAAAGGCATCC-3';

mouse *Xbp1t*, forward primer 5'-TGGCCGGGTCTGCTGAGTCCG-3' and reverse primer 5'-GTCCATGGGAAGATGTTCTGG-3';

mouse *Xbp1s*, forward primer 5'-CTGAGTCCGAATCAGGTGCAG-3' and reverse primer 5'-GTCCATGGGAAGATGTTCTGG-3';

mouse *Chop*, forward primer 5'-CTGGAAGCCTGGTATGAGGAT-3' and reverse primer 5'-CAGGGTCAAGAGTAGTGAAGGT-3';

mouse *Dr5*, forward primer 5'-GCAGAGAGGGTATTGACTACACC-3' and reverse primer 5'-GCATCGGGTTTCTACGACTTT-3';

mouse *Trb3*, forward primer 5'-*TGCAGGAAGAAACCGTTGGAG*-3' and reverse primer 5'-CTCGTTTTAGGACTGGACACTTG-3';

mouse *Gapdh*, forward primer 5'-GGATTTGGCCGTATTGGG-3' and reverse primer 5'-GTTGAGGTCAATGAAGGGG-3';

mouse *Bloc1s1*, forward primer 5'-TCCCGCCTGCTCAAAGAAC -3' and reverse primer 5'- GAGGTGATCCACCAACGCTT-3';

mouse *c-Myc*, forward primer 5'-ATGCCCCTCAACGTGAACTTC-3' and reverse primer 5'-GTCGCAGATGAAATAGGGCTG-3';

mouse *c-Fos*, forward primer 5'-TTGAGCGATCATCCCGGTC-3' and reverse primer 5'-GCGTGAGTCCATACTGGCAAG-3';

mouse *Hif1a*, forward primer 5'-GTCCCAGCTACGAAGTTACAGC-3' and reverse primer 5'-CAGTGCAGGATACACAAGGTTT-3'.

This article is protected by copyright. All rights reserved.

Author Manuscript

Luciferase reporter assay

To measure NF-κB activation, the luciferase (Luc) reporter plasmid was generated by inserting into the pGL3-Basic plasmid (Promega Corp., Madison, WI) a basic promoter element (TATA box) joined to a tandem repeat of NF-κB binding elements. HepG2 cells were co-transfected for 48 hours with the Luc reporter construct and pRL-TK renilla plasmid (Promega Corp., Madison, WI), along with siRNAs against IRE1α or XBP1 or a scramble control siRNA. Cells were then treated with TNFα for 24 hours, and luciferase activity was measured using the Dual-Luciferase Reporter Assay System (Promega Corp., Madison, WI) according to the manufacturer's instructions. The oligonucleotide siRNAs used are as follows:

siIRE1α-#1: sense 5'-GGAGAGAAGCAGCAGACUUdTdT-3' and antisense 5'-AAGUCUGCUGCUUCUCUCCdTdT-3';

siIRE1α-#2: sense 5'-GCGUAAAUUCAGGACCUAUdTdT-3' and antisense 5'-AUAGGUCCUGAAUUUACGCdTdT-3');

Scramble control siRNA for siIRE1α: sense 5'-CGUACGCGGAAUACUUCGAdTdT-3' and antisense 5'-UCGAAGUAUUCCGCGUACGdTdT-3';

siXBP1-#1: sense 5'-CCAGUCAUGUUCUUCAAAUTT-3' and antisense 5'-AUUUGAAGAACAUGACUGGTT-3';

siXBP1-#2: sense 5'-GGAACAGCAAGUGGUAGAUTT-3' and antisense 5'-AUCUACCACUUGCUGUUCCTT-3';

Scramble control siRNA for siXBP1: sense 5'-UUCUCCGAACGUGUCACGUTT-3' and antisense 5'-ACGUGACACGUUCGGAGAATT-3'.

Clinical HCC specimens and tissue microarray analysis

With the written informed consent from the patients, twelve pairs of human HCC tissues and their corresponding adjacent non-tumor tissues that were at least 3 to 4 cm away from the tumor, were obtained from the Eastern Hepatobiliary Surgery Hospital. The fresh specimens were snap-frozen in liquid nitrogen and stored at -80°C until further analysis. The experimental protocol was approved by the Institutional Ethical Review Board at the Institute for Nutritional Sciences, Chinese Academy of Sciences.

This article is protected by copyright. All rights reserved.

HCC tissue microarrays, collected from 94 HCC tissues with matched non-HCC liver tissues close to the tumor, were prepared and immunostained with the anti-IRE1α antibody (#ab96481, Abcam, Cambridge, MA) and anti-phospho-STAT3 antibody (#8204, CST, Danvers, MA) by the Biochip Shanghai National Engineering Research Center. The collection and use of these human clinical samples were approved by the Ethical Committee of Taizhou Hospital, Zhejiang, China. IHC scoring was performed by a clinical pathologist according to the histological scoring system (H-score), which was based on the IHC staining intensity (0, no staining; 1, low; 2, moderate; and 3, high) and the percentage of stained cells (0, 0; 1, 1-25%; 2, 25-50%; 3, 51-75% and 4, 76-100%). Expression levels of IRE1α protein and phosphorylated STAT3 in each HCC tissue was designated as either low (H-score ≤4) or high (H-score >4).

References

1. Shao M, Shan B, Liu Y, Deng Y, Yan C, Wu Y, Mao T, et al. Hepatic IRE1alpha regulates fasting-induced metabolic adaptive programs through the XBP1s-PPARalpha axis signalling. Nat Commun 2014;5:3528.

2. Liu Y, Shao M, Wu Y, Yan C, Jiang S, Liu J, Dai J, et al. Role for the endoplasmic reticulum stress sensor IRE1alpha in liver regenerative responses. J Hepatol 2015;62:590-598.

3. Verna L, Whysner J, Williams GM. N-nitrosodiethylamine mechanistic data and risk assessment: bioactivation, DNA-adduct formation, mutagenicity, and tumor initiation. Pharmacol Ther 1996;71:57-81.

4. Xia J, Zhou Y, Ji H, Wang Y, Wu Q, Bao J, Ye F, et al. Loss of histone deacetylases 1 and 2 in hepatocytes impairs murine liver regeneration through Ki67 depletion. Hepatology 2013;58:2089-2098.

5. Kim H, Choi GH, Na DC, Ahn EY, Kim GI, Lee JE, Cho JY, et al. Human hepatocellular carcinomas with "Stemness"-related marker expression: keratin 19 expression and a poor prognosis. Hepatology 2011;54:1707-1717.

This article is protected by copyright. All rights reserved.

Author Manuscript

6. Ghosh R, Wang L, Wang ES, Perera BG, Igbaria A, Morita S, Prado K, et al. Allosteric inhibition of the IRE1alpha RNase preserves cell viability and function during endoplasmic reticulum stress. Cell 2014;158:534-548.

7. Volkmann K, Lucas JL, Vuga D, Wang X, Brumm D, Stiles C, Kriebel D, et al. Potent and selective inhibitors of the inositol-requiring enzyme 1 endoribonuclease. J Biol Chem 2011;286:12743-12755.

8. Cross BC, Bond PJ, Sadowski PG, Jha BK, Zak J, Goodman JM, Silverman RH, et al. The molecular basis for selective inhibition of unconventional mRNA splicing by an IRE1-binding small molecule. Proc Natl Acad Sci U S A 2012;109:E869-878.

9. Qi L, Yang L, Chen H. Detecting and quantitating physiological endoplasmic reticulum stress. Methods Enzymol 2011;490:137-146.

Author Manuscript

This article is protected by copyright. All rights reserved.

Author Manuscript

Figures

Fig. S1

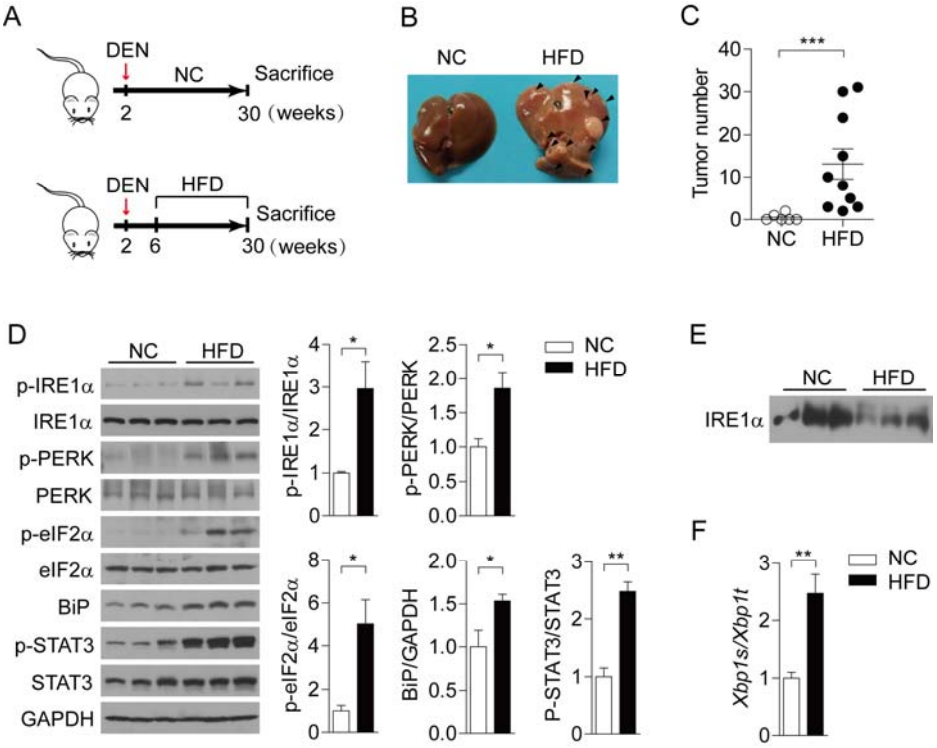

Fig. S1. Promotion by dietary obesity of HCC is accompanied by hepatic ER stress. Two-week-old male C57BL/6 mice were i.p. injected with DEN (50 mg/kg body weight) and were maintained on a normal-chow (NC) diet (n=6), or fed a high-fat diet (HFD) beginning at 6 weeks of age (n=10). Mice were sacrificed at 30 weeks of age. (**A**) Schematic of the experimental design. (**B**) Representative images of mouse livers from the indicated group. Tumors are indicated by arrows. (**C**) The numbers of liver tumors. (**D**) Immunoblot analysis of phosphorylation of IRE1α, PERK, eIF2α and STAT3 as well as BiP protein expression from liver extracts. Representative results are shown for three individual mice per group. GAPDH was used as the loading control. Shown also are results from densitometric quantification of the immunoblots after normalization to that of NC-fed mice. (**E**) Representative phos-tag gel for immunoblot analysis of IRE1α protein. (**F**) Quantitative RT-PCR analysis of *Xbp1* mRNA splicing. Data in (**C**, **D**, **F**) are presented as the mean ± s.e.m., **P* < 0.05, ***P*<0.01, ****P*<0.001 by two-tailed unpaired Student's *t*-test.

This article is protected by copyright. All rights reserved.

Author Manuscript

Fig. S2

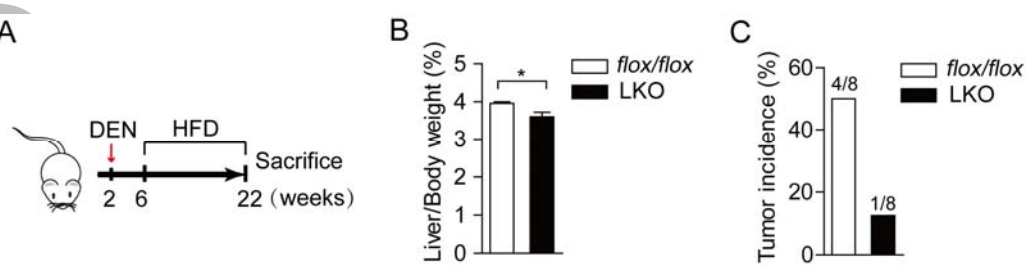

Fig. S2. Hepatocyte IRE1α ablation blunts dietary obesity-accelerated HCC development. Two-week-old male LKO mice and their *flox/flox* littermates were i.p. injected with DEN (50 mg/kg body weight) and were maintained on an HFD beginning at 6 weeks of age (n=8 per genotype). Mice were sacrificed at 22 weeks of age for HCC analysis. (**A**) Schematic of the experimental design. (**B**) Ratios of liver weight to body weight. (**C**) Incidence of HCCs. Data are shown as the mean ± s.e.m., **P* < 0.05 by two-tailed unpaired Student's *t*-test.

This article is protected by copyright. All rights reserved.

Author Manuscript

Fig. S3

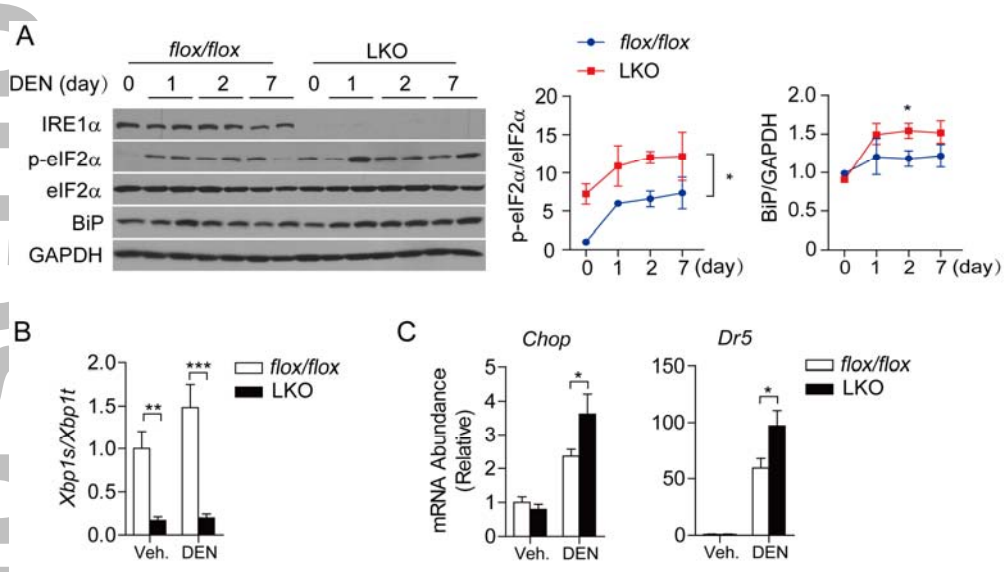

Fig. S3. Abrogation of hepatocyte IRE1α promotes DEN-induced activation of the eIF2α-CHOP branch of ER stress. Four-week-old *flox/flox* and LKO mice were administrated with DEN (100 mg/kg body weight) or saline (vehicle) and were sacrificed at the indicated time after injection (n=5 per group). (**A**) Immunoblot analysis of eIF2α phosphorylation and BiP protein in liver extracts. GAPDH was used as the loading control. Densitometric quantification of eIF2α phosphorylation and BiP protein levels are shown after normalization to the value of untreated *flox/flox* mice. (**B, C**) Quantitative RT-PCR analysis of *Xbp1* mRNA splicing (**B**) and the mRNA abundance of *Chop* and *Dr5* (**C**) in livers of mice at 2 days after DEN administration. Data are shown as the mean ± s.e.m., **P* < 0.05, ***P*<0.01 by two-tailed unpaired Student's *t*-test or two-way ANOVA.

This article is protected by copyright. All rights reserved.

Author Manuscript

Fig. S4

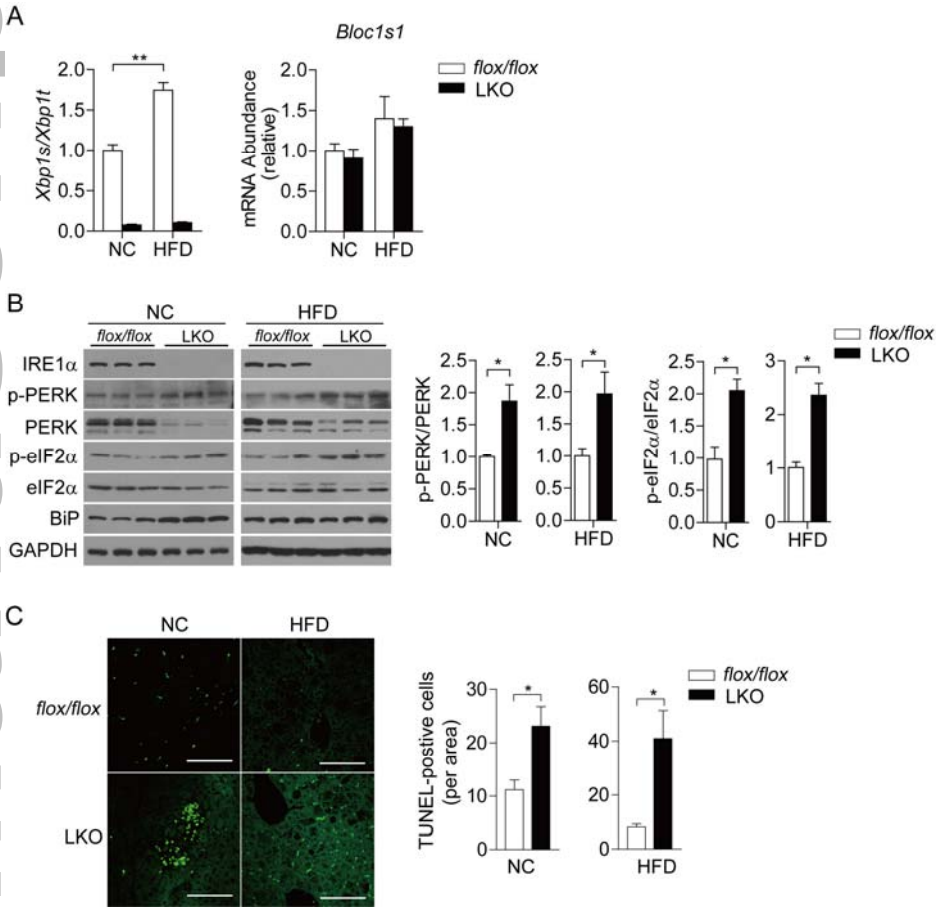

Fig. S4. Hepatocyte IRE1α ablation leads to increased hepatic ER stress and apoptosis in DEN-treated mice. Two-week-old male LKO and *flox/flox* mice were injected with DEN and then maintained on an NC for 40 weeks, or fed an HFD for 24 weeks, starting at 6 weeks of age (n=8 per group). (**A**) Quantitative RT-PCR analysis of *Xbp1* mRNA splicing and the mRNA abundance of *Bloc1s1* in the livers. (**B**) Immunoblot analysis of phosphorylation levels of PERK and eIF2α as well as BiP protein levels from liver extracts. Representative immunoblots are shown for three individual mice per group. Shown also are densitometric quantification results after normalization to those of *flox/flox* mice. (**C**) Analysis of apoptosis in liver sections. Shown are representative TUNEL labeling images (6 images per liver) and quantifications of TUNEL-positive cells (n=5 per group). Scale bars, 100 μm. Data are shown as the mean ± s.e.m, **P* < 0.05 by two-tailed unpaired Student's *t*-test.

This article is protected by copyright. All rights reserved.

Author Manuscript

Fig. S5

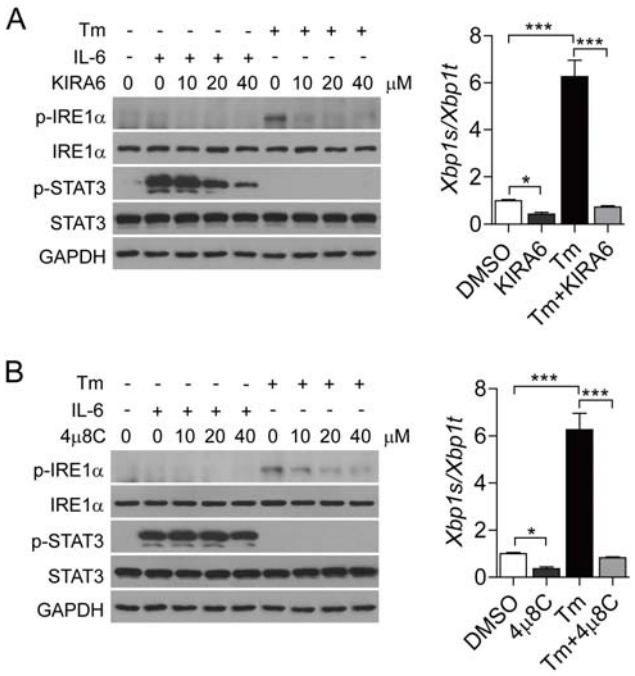

Fig. S5. Blocking IRE1α's kinase but not RNase activity attenuates IL-6-induced STAT3 phosphorylation. HepG2 cells were pretreated with DMSO (-) versus KIRA6 (**A**) or 4μ8C (**B**) for 30 min at the indicated concentrations and then stimulated with IL-6 (10 ng/ml) for another 30 min. Shown are representative immunoblot analyses of IRE1α and STAT3, along with quantitative RT-PCR analysis of *Xbp1* mRNA splicing. Cells likewise treated with tunicamycin (Tm, 10 ng/ml) for another 2 hr were used as the control experiment. Data from 3 independent experiments are presented as the mean ± s.e.m., **P* < 0.05, ****P*<0.001 by one-way ANOVA.

This article is protected by copyright. All rights reserved.

Author Manuscript

Fig. S6

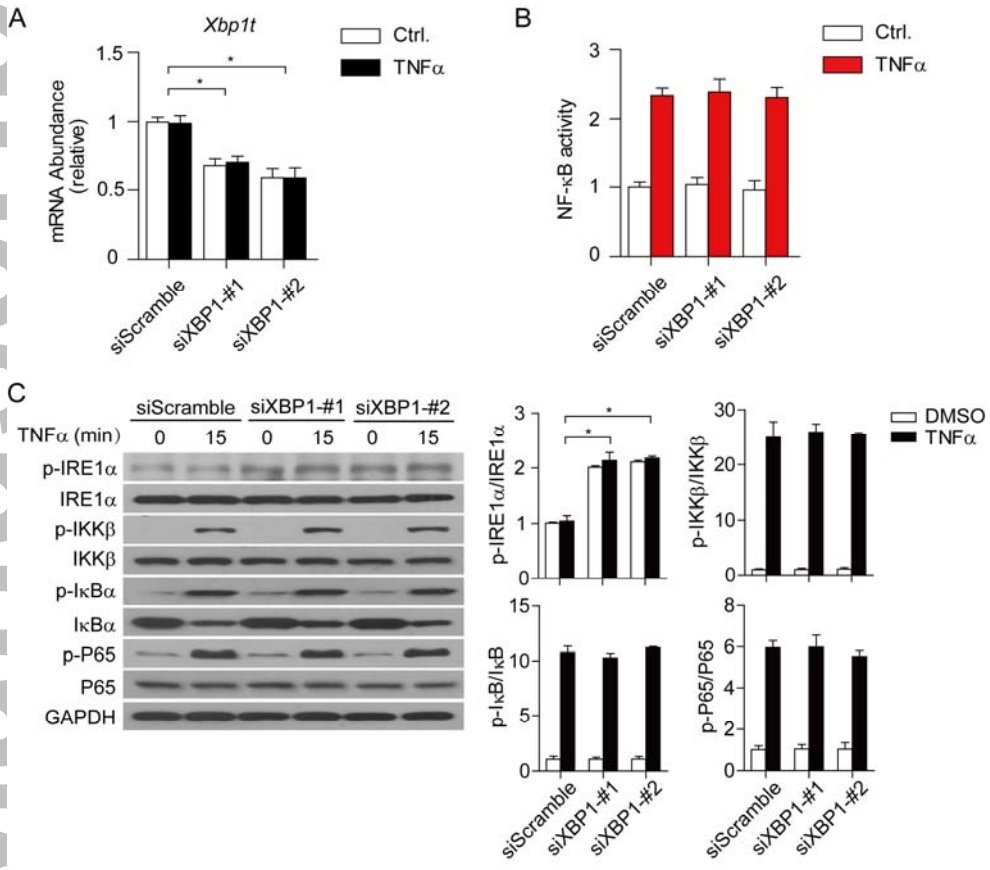

Fig. S6. Knockdown of XBP1 expression does not affect TNFα activation of the IKKβ-NF-κB pathway. (**A**) HepG2 cells were transfected for 48 hours with two siRNAs directed against *Xbp1* or a scramble control. Cells were then treated with TNFα (10 ng/ml) for 24 hours. Quantitative RT-PCR analysis of *Xbp1* mRNA abundance for assessment of knockdown efficiency. (**B**) HepG2 cells were co-transfected for 48 hours with the NF-κB-luciferase reporter plasmid along with *Xbp1* siRNAs or the scramble control. Cells were then treated with TNFα (10 ng/ml) for 24 hours, and NF-κB activity was determined by the luciferase assay. Shown are relative luciferase activities after normalization to renilla that was used as the internal control. (**C**) HepG2 cells were transfected with the scramble or *Xbp1* siRNAs and then treated with TNFα (10 ng/ml) for 15 min. Phosphorylation of IKKβ, IκBα and P65 proteins was analyzed, and data are shown after normalization to the value of the untreated control cells. Results from 4 independent experiments are presented as the mean ± s.e.m., $*P < 0.05$ by two-way ANOVA.

This article is protected by copyright. All rights reserved.